nature communications

Article

https://doi.org/10.1038/s41467-025-59559-8

Edible aquatic robots with Marangoni propulsion

Received: 10 October 2024

Accepted: 23 April 2025

Published online: 07 May 2025

Check for updates

Shuhang Zhang[1], Bokeon Kwak[1], Ruihao Zhu[2], Markéta Pankhurst[1], Lu Zhang[2], Remko M. Boom[2] & Dario Floreano[1]

Centimeter-scale aquatic robots could be used in environmental monitoring, exploration, and intervention in aquatic environments. However, existing robots rely on artificial polymers and commercial electronic components, which can pollute and disrupt sensitive ecological environments if they are not retrieved. To address these challenges, we describe a fully biodegradable and fully edible self-propelled device that leverages the Marangoni effect for autonomous propulsion. The body of the edible aquatic robot is made of freeze-dried fish food and is powered by a water-triggered pneumatic reaction that produces motion by sustained release of a surfactant that is safe for aquatic fauna. The device's biodegradable and non-toxic composition allows for safe environmental deployment for environmental sensing, delivery of nutrition or medication in aquatic environments. The proposed method substantially expands the potential benefits of small-scale aquatic robots that could be deployed on a large scale without the need to retrieve them and even provide nutrition to wildlife at the end of their lifetime as animals do.

Aquatic robots have a wide range of applications in exploration, monitoring, and intervention missions within natural environments[1–3]. In particular, there has been growing interest in centimeter-scale aquatic robots due to their compact size, low power consumption, minimal environmental impact, and suitability for navigating confined and complex natural water bodies[4,5]. Various actuation mechanisms—including piezoelectric actuators[6,7], dielectric elastomer or hydraulic actuation[5,8], electricity-driven hydrogels[9], or miniatured DC motors[10]—have been employed, enabling locomotion by means of diverse propulsion methods such as undulation[5,8], vibration[10], direct jetting[6] or stroking[7,9]. When integrated with miniaturized power sources and driving circuits, these robots can display untethered, highly maneuverable movement[5,8–10] with speeds between one and three times their body length per second while consuming power in the range of tens to hundreds of microwatts[5,7,9].

However, existing robots are predominantly constructed from artificial plastic polymers and commercial electronic components, including electrical batteries. While these materials may be harmless if the robots are retrieved after completing their task, they pose risks to natural environments if they are lost or ingested by wildlife.

Self-propulsion by the Marangoni effect[11]—whereby a floating body is propelled by the ejection of surfactant chemicals that locally decrease the water surface tension—can offer an alternative to electrical power sources and control circuits. Recent advancements in Marangoni-effect-driven self-propelled devices have led to innovations such as imbibition microfluidic pumps[12], pen-drawn actuators[13], programmable gels[14], and biodegradable protein motors[15] that facilitate self-propelled locomotion. Additionally, on-the-fly control of Marangoni propulsion robots has been demonstrated through remote photothermal switching[16]. However, current approaches remain unsuitable for outdoor aquatic environments because they typically rely on surfactants, such as alcohol[14] or other potentially toxic chemicals[12,13], which can be harmful to aquatic organisms. Furthermore, bodies and ejection structures of those robots are often non-biodegradable, limiting their applicability in ecologically sensitive

[1]Laboratory of Intelligent Systems, School of Engineering, École Polytechnique Fédérale de Lausanne, STI-IGM-LIS, Lausanne, Switzerland. [2]Laboratory of Food Process Engineering, Wageningen University and Research, Wageningen, The Netherlands. e-mail: dario.floreano@epfl.ch

scenarios where transient and biodegradable properties are required[17,18].

Here, we present a method for designing, modeling, and fabricating a fully biodegradable and edible self-propelled aquatic robot. The cm-scale aquatic robot is composed of a water-triggered switch that initiates a chemical reaction within the robot's belly when placed on a water surface; the chemical reaction produces gas that gradually expels a surfactant into the water from the rear of a milli-fluidic reservoir, thus generating a sustained motion. The robot could be functionalized with edible sensors[17,19] and deployed in large numbers for environmental monitoring over large areas[20]; also, the nutritional profile of its body could be tailored to serve as a nutrient or medical treatment for specific aquatic fauna (Fig. 1a).

Results

Design and modeling

The aquatic robot, endowed with water-sensing, energy storage and production, and self-propelling capabilities, consists of a multi-layered structure made of entirely edible materials for aquatic fauna (Fig. 1b). The operating principle (Fig. 1c) consists of the gradual release of a surfactant pushed out of the pellet by gas pressure, generated by a chemical reaction triggered shortly after the pellet is placed on water surface. The aquatic robot is made of two structures: (1) a boat-shaped body, which provides buoyancy and directional motion, and serves as the main source of nutrition as a showcase in this work; (2) a fluidic actuator to generate motion that includes a reservoir of liquid surfactant (fuel) and a detachable chemical reaction chamber (Fig. 1c) with powdered chemicals (citric acid and sodium bicarbonate), which produce gas by reacting with water. Once the aquatic robot is deployed on the water surface, the permeable bottom of the fluidic actuator will start absorbing water and trigger a reaction between citric acid and sodium bicarbonate, generating CO_2, which will in turn push the fuel out of the reservoir, thus reducing the water surface tension behind the aquatic robot and producing forward motion (Fig. 1d). Citric acid and sodium bicarbonate materials are not only well-characterized sources of pneumatic power in soft robotics[21,22] but are also safe to consume by aquatic fauna and are commonly used in aquafarming as feed additives and functional chemicals[23–25]. Besides CO_2, another byproduct of the chemical reaction is sodium citrate, which has also been studied as an aquatic feed ingredient[26–28] where a concentration up to 1% of feed by mass is considered safe.

For the sake of simplicity, in this work we consider only locomotion time and speed, although directional change comes for free from manufacturing imperfections and fluid dynamics, as we will show below. In terms of motion duration, here we target a motion duration of a few minutes, sufficient to gather and transmit data from a given sensor (temperature, pH, e.g.), as a proof of concept. Assuming that the aquatic robot acts as prey at the end of its lifetime, we considered the preferred swimming speeds of several typical aquatic species, which range from 0.5 to 3 body lengths per second (bl·s^{-1})[29]. We thus assume that a small aquatic robot capable of approximating that speed range could be considered prey. To predict locomotion speed and duration, and thus assess the performance of the manufactured aquatic robot, we developed a simple physical model based on the literature[30] (Supplementary Methods Section S1 and Fig. S1).

Hull structure

The boat-shaped body of the aquatic robot is made of materials obtained from commercial fish feed pellets. Most commercial pellets are near spherical or cylindrical with a diameter up to 14 mm[31], depending on the target fish species and age, and contain all ingredients for a complete diet (18–50 percents protein, 10–25 percents lipids, 15–20 percents carbohydrate, up to 8.5 percents ash (including minerals), up to 1.5 percents phosphorus and trace amounts of vitamins[32]). Since mass m and drag coefficient c_d (Supplementary

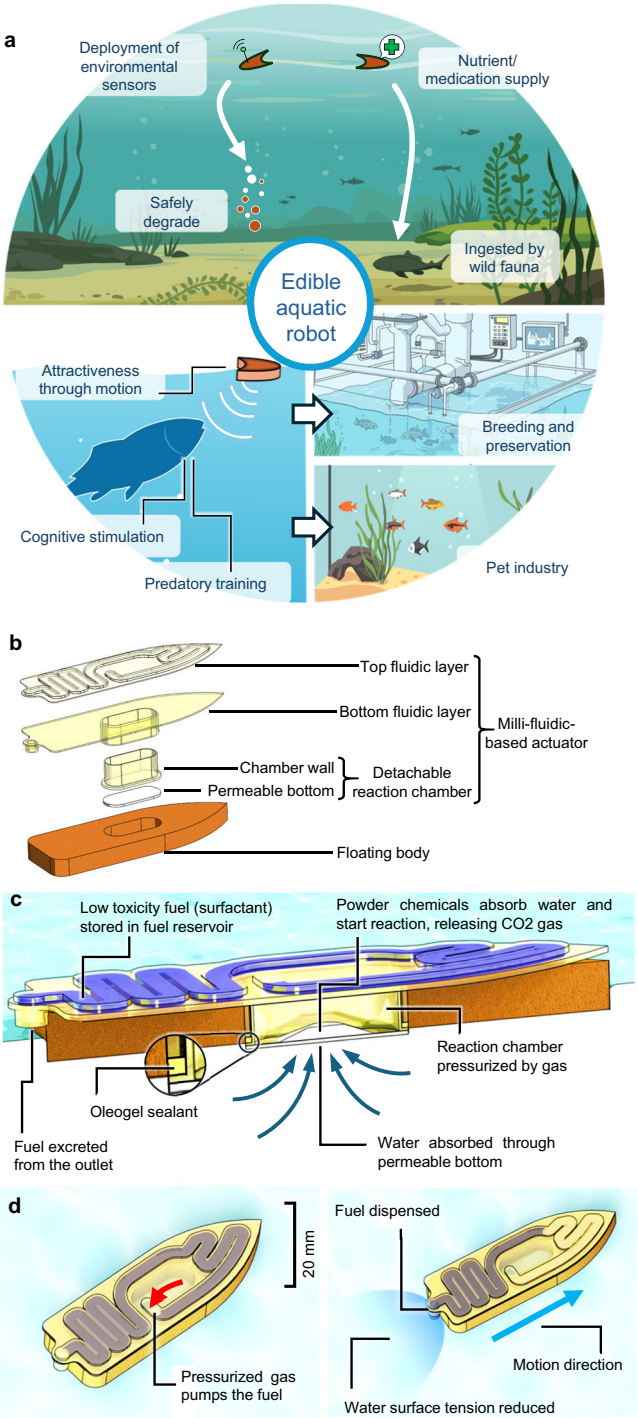

Fig. 1 | Edible aquatic robot concept, design, and work principle. a Future application scenarios of edible aquatic robots. **b** The multilayer structure of the aquatic robot made from edible materials, which comprises a boat-shaped body to provide buoyancy and various nutrients, and a fluidic actuator that encloses the fuel reservoir and the reaction chamber. **c** Sectioned structure view and working principle of the fluidic actuator. Only upon contact with the water surface, the effervescent reaction will be triggered and produce the gas pressure that allows the fuel to be dispensed through the outlet. The oleogel sealant is applied to guarantee an airtight fit between the reaction chamber and bottom fluidic layer, which is crucial for the functioning of the device. **d** Top view of the fuel dispensing and propulsion procedure. The fuel decreases the liquid surface tension behind the aquatic robot, creating the tension gradient that drives forward motion.

https://doi.org/10.1038/s41467-025-59559-8

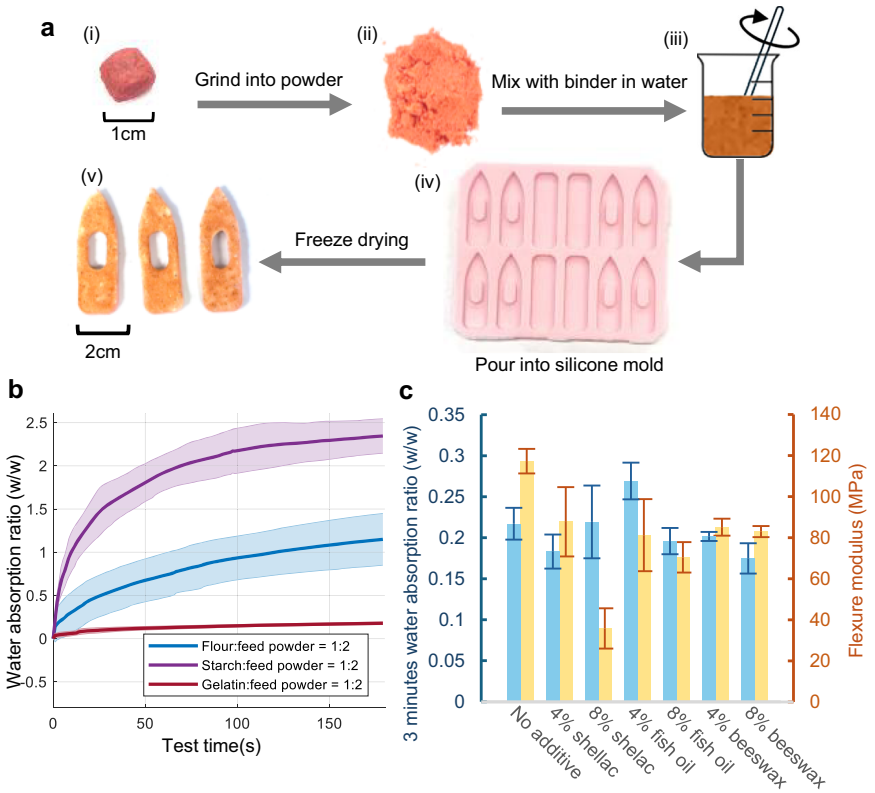

Fig. 2 | Manufacture and testing of boat-shaped body samples. a Manufacturing process of boat-shaped body samples. (i) Commercial feed pellets (approximate density 0.7 g/m^3) were first ground into powder for reshaping. (ii) The powder was then mixed with the selected binder and, optionally, hydrophobic additives in water. (iii) The mixture was heated to 90 °C and stirred to disperse the components evenly. (iv) The mixture was then poured into silicone molds to shape hulls and rectangular bars for bending tests. (v) The samples were frozen, removed from the mold, and subjected to freeze-drying to remove all the water and produce the final porous structure. **b** Water absorption results of recipes based with three different binders (starch, flour, and gelatin); legend indicates material mass ratios in each recipe. **c** Comparison of water absorption ratio (blue bars) and flexure modulus (yellow bars) of seven recipes with different types and quantity of hydrophobic additives: shellac, fish oil, and beeswax. A higher water absorption ratio corresponds to less water resistance, which is not desirable for the aquatic robot. The flexure modulus reflects the material's strength against bending load, which is used as an indicator of the material's structural integrity. Error bars show the standard deviation of tests on three separate samples.

Methods Section S1) negatively impact the boat's propulsion speed, the material density should be as low as possible while maintaining structural integrity. Here we aimed for a density of 250 kg/m^3 because it is similar to the lowest density of commercial floating pellets (reported to be 267–711 kg/m^3)[33]. We designed streamlined hull shapes with an estimated drag coefficient between 0.76 to 1.60 to support target speeds of 3–0.5 body lengths per second (Supplementary Methods Section S2), where larger drag coefficients correspond to lower motion speeds and lower Reynolds numbers.

Commercial feed pellets were ground to powder, mixed with a polymer binder to ensure structural integrity of the final product, poured into a boat-shaped mold, and freeze-dried (Fig. 2a). Freeze-drying was used because it can reliably produce lightweight yet strong structures[34]. However, freeze-dried food items display high porosity, which would lead to rapid water absorption that would increase the hull's density and reduce motion capability. To address this issue, three common edible binders (starch, flour, and gelatin) were separately combined with the ground pellets and compared against dynamic water uptake within 3 min; in addition, texture analysis with flexure modulus was measured to assess structural integrity of the freeze-dried structures. All the freeze-dried samples had an average density of 250 ± 13 kg/m^3 and a mass of 0.50 g ± 0.03 g.

The recipe with gelatin binder displayed a water absorption rate five times lower than the other two recipes within a 3-min time window (Fig. 2b), which is desirable to maintain the lightweight and structural integrity of the device. To further improve water resistance, several edible waterproof additives (shellac, fish oil, and beeswax), each tested in 4% and 8% of total dry mass, were added during the mixing process (Fig. 2a(ii, iii)) and the resulting freeze-dried structures were compared for water absorption ratio and flexure modulus. However, these additives did not show substantial improvements in water absorption ratios (Fig. 2c, left vertical axis) and even reduced the flexural modulus (Fig. 2c, right vertical axis), which is a measure of structural integrity. Therefore, we did not use these additives and resorted to a recipe made only of ground feed pellets and gelatin to produce boat-shaped samples with a mass of 0.49 g ± 0.02 g, an average flexure modulus of 117.28 MPa, and a maximum load of 24.72 N similar to the crushing load of commercial fish feed pellets, which range between 6 and 33 N[33].

Fuel selection

There are several types of surfactant materials (volatile smaller molecules, non-volatile amphiphilic molecules or polymers, either in solid or liquid form) with diverse water solubility and surface-tension reduction. Within the scope of an application in aquatic environments, the surfactant should not only provide the highest surface-tension reduction but also display the lowest toxicity for aquatic species. Some surfactants have already been used for Marangoni-based propulsion of non-edible artefacts, such as butanol[12], camphor[13], hexafluoro-isopropanol[15], sodium dodecyl sulfate[35], and ethanol[36], but most of these are toxic to aquatic animals. Here, we select a range of surfactants that are known as food additives. and propose an approach to compare their environmental impact by establishing a toxicity index I_{toxic} from standard

https://doi.org/10.1038/s41467-025-59559-8

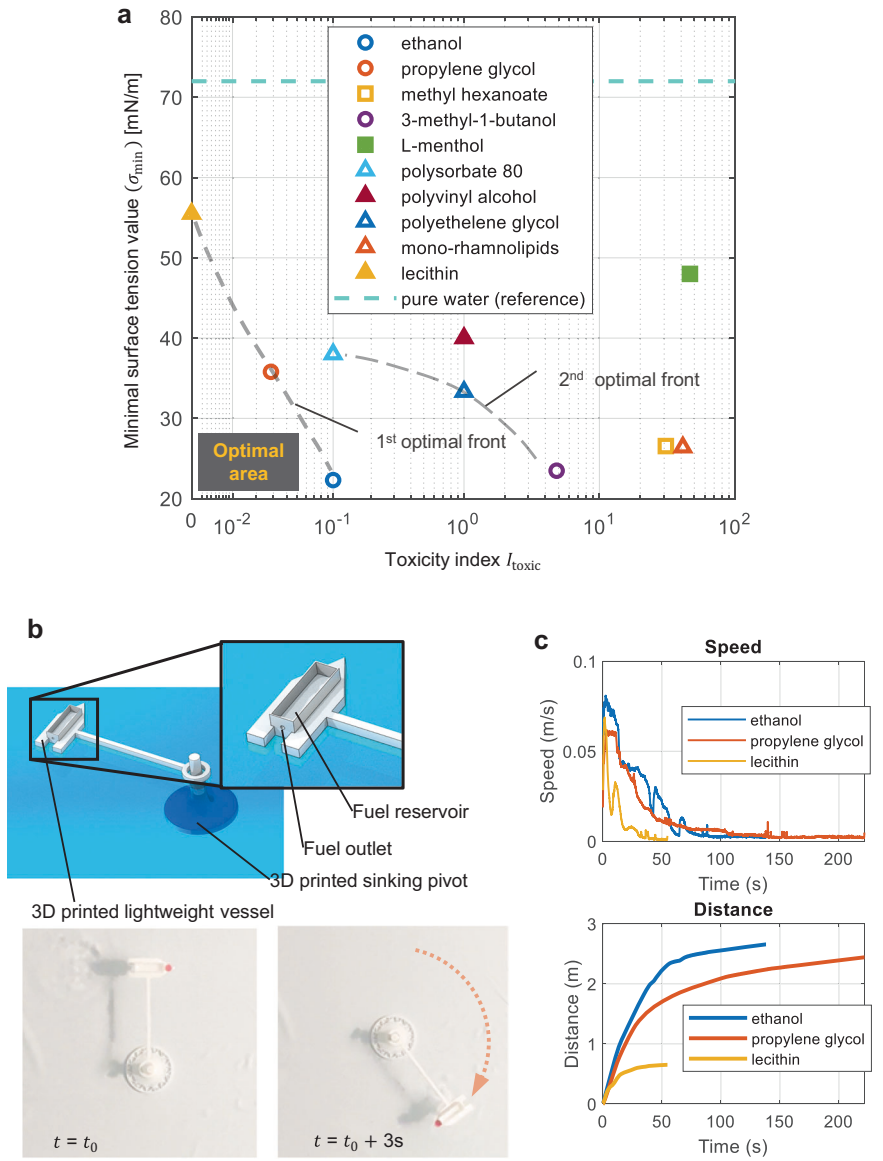

Fig. 3 | Selection of fuel by toxicity and propulsion ability. a Comparison of various edible fuel candidates according to their minimal surface tension σ_{min} when mixed with water and toxicity index value I_{toxic}. Circular or square symbols denote volatile small molecules with high or low solubility, respectively, while triangular symbols represent larger amphiphilic molecules or polymers. Filled symbol indicates solids at room temperature (297 K) and 1 atm, whereas empty symbols denote liquid. **b** Experimental setup for comparing the motion capabilities of liquid fuels. **c** Comparison of speed and traveled distance with lecithin, propylene glycol, and ethanol.

environmental toxicity data, namely "half maximal effective concentration" (EC50) and "no observed effect concentration" (NOEC) values[37,38] (Supplementary Methods Section S3), and assess their surfactant performance in a standardized manner. Higher EC50 or NOEC values correspond to lower toxicity and thus to a lower toxicity index. Unfortunately, the surfactant toxicity reported in the literature is often measured on one or a few species, which vary in their tolerance to the substance. To illustrate our comparison method, here we use published toxicity data for freshwater flea (*Daphnia magna*) because this organism has been used in the largest number of studies[39–46], and we assume that the resulting toxicity index rank applies to fish too. However, the proposed method is also applicable to any other aquatic species for which toxicity data of multiple surfactants exist. For the edible surfactant lecithin, there is no NOEC or EC50 data because it is considered safe for the aquatic environment[47]; in this case, the toxicity index is defined as 0.

Since surface-tension reduction (evaluated by the minimal surface tension σ_{min} of surfactant-water mixture, sourced from literature[48–57]) and toxicity (evaluated by toxicity index I_{toxic}) are not directly comparable, the results identify a Pareto-optimal front that includes lecithin, propylene glycol, and ethanol (Fig. 3a).

To assess the propulsion performance of lecithin, propylene glycol, and ethanol, we developed a rotary motion test rig, which comprises a lightweight, 3D-printed plastic vessel floating on water that moves around a pivot (Fig. 3b). 0.3 g of each fuel was used for each test: propylene glycol and ethanol in pure form, and lecithin in liquid dispersion form as purchased (see "Methods" section). Each fuel was injected into the fuel reservoir, and the vessel was released onto the water surface while its motion was recorded by video. We observed that lecithin, despite being the safest edible surfactant, quickly saturated the water surface due to its low solubility and amphiphilic nature, reducing motion time of the edible aquatic robot (Fig. 3c), and

https://doi.org/10.1038/s41467-025-59559-8

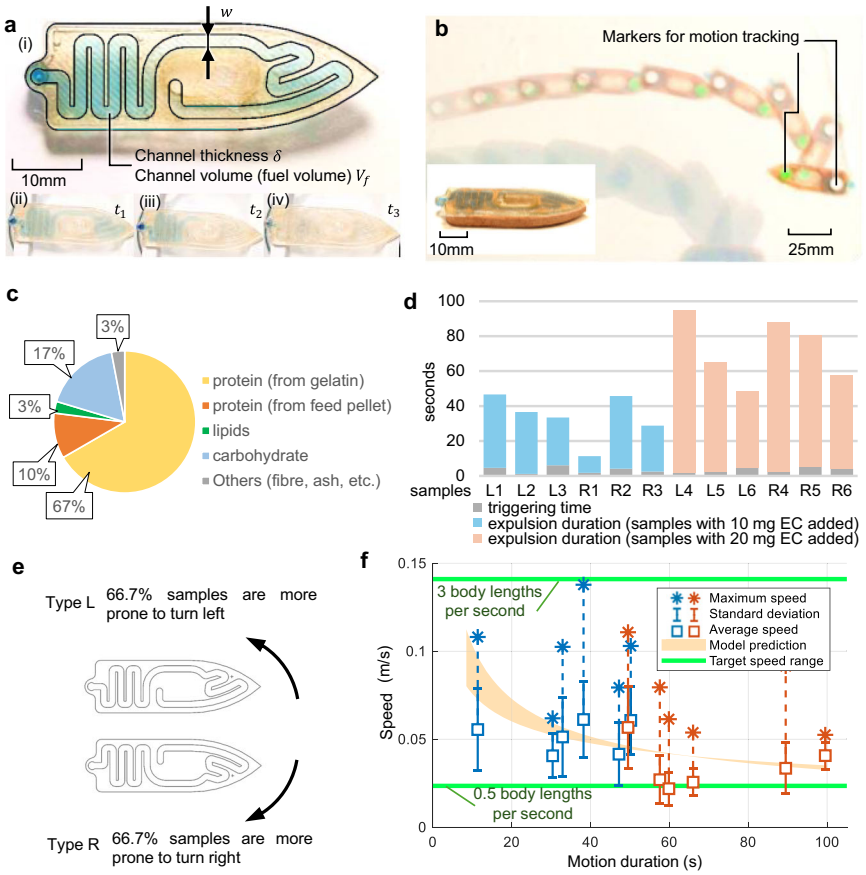

Fig. 4 | Characterization of the edible aquatic robot. a Fluidic actuator design and fuel expulsion process. (i) Fluidic actuator with injected fuel photograph, blue food dye was added to the fuel for visualization. The fluidic actuator's shape and size parameters were illustrated with additional black lines. (ii–iv) Illustration of the exhaustion of the fuel reservoir by time (t_1<t_2<t_3). The fuel expulsion is triggered by water and driven by the gas pressure generated from the chemical reaction. **b** Sample trajectory of an edible aquatic robot captured during motion tests. **c** Nutritional profile of the edible aquatic robot based on the material composition of the boat-shaped body and of the fluidic actuator. **d** Triggering time and expulsion duration of 12 fluidic actuator samples, where L1–L6 represent the 6 samples of type L, R1–R6 represent the six samples of type R. **e** Asymmetric trend of turning direction of the edible aquatic robots with the two types of samples, likely caused by the asymmetricity of the design. **f** Comparison of motion velocity and duration predicted by the model with those measured in experiments. Blue and orange data points represent edible aquatic robot samples that contain 10 mg and 20 mg ethylcellulose powder in their reaction chambers, respectively.

therefore we narrowed the fuel selection to propylene glycol and ethanol, which are both highly soluble and therefore allow prolonged motion.

The energy provided by the two types of fuel for locomotion can be measured by integrating over time the product of the driving force F_s and velocity u (Supplementary Methods Section S5) measured during the tests (Fig. 3c). This results in a total motion energy of 1.07×10^{-4} J for propylene glycol and 1.94×10^{-4} J for ethanol. Although propylene glycol provided only 55.11% of the motion energy produced by ethanol, the latter is more toxic to aquatic species and has a safety concentration limit (evaluated by the 48 h EC50[39,40] for *Daphnia magna*) that is only 28.37% of that for propylene glycol. Therefore, propylene glycol, which has also been proven safe as a feed additive in aquafarming[58], was selected as the fuel for the edible aquatic robot.

Fluidic actuator

The fluidic actuator (Fig. 1d) is designed to host the fuel (propylene glycol) and a reaction chamber sealed by a permeable membrane that triggers gas generation when positioned on water to push the fuel out of the reservoir. It consists of a shell structure composed of two layers (Fig. 1c): the top layer, which holds the fuel reservoir, and the bottom layer, which holds the reaction chamber and the water-permeable membrane. Both layers are made of gelatin, a material with nutritional value[59] and well-tested methods for the production of millimeter-scale capsules[60], by pouring and drying in silicone molds. The average mass of the fluidic actuator samples was 0.603 g, excluding the fuel- and gas-generation chemicals.

The fuel reservoir (Fig. 1d) consists of a single fluidic channel with a waving pattern designed to maximize fuel capacity and smooth expulsion (Supplementary Methods Section S5). This necessarily led to an asymmetric configuration. To analyze the potential effects of this asymmetricity, two types of actuators: type L and type R, which have mirrored designs, have been fabricated for comparison. The channel has a width $w = 1.8$ mm and thickness $\delta = 0.8$ mm (Fig. 4a), resulting in a nominal volume $V_f = 195$ μl, which represents the maximum payload to keep the fuel outlet above the water surface. Due to shrinkage of the gelatin material during the fabrication process, resulting in a decreased volume of the fuel reservoir, the actual average volume of fuel injected in the reservoir of the samples was 151.7 μl.

The reaction chamber contained sodium bicarbonate and citric acid as active reagents (Fig. 1d). To achieve the target speed of 0.5–3 body lengths per second (bl·s^{-1}), which corresponds to 23.5–141 mm/s for vessels with a length of 47 mm, the required fuel flow rate q was estimated to be between 1.00 and 29.96 μl/s (Supplementary Methods Section S5). In this study, we used 10 mg (5.21×10^{-5} mol) of citric acid and 10 mg (11.90×10^{-5} mol) of sodium bicarbonate in each vessel (Supplementary Methods Section 5) to achieve the desired gas-generation rate between 3.84 and 23.02 μl/s, depending on the

amount of absorbed water. Our approach was based on a previous study[22] of gas-generation rate for varying concentrations of sodium bicarbonate and citric acid, while also considering the requirement for the resulting sodium citrate not exceeding the safety limit of 1% of the total feed mass (see subsection "Design and modeling"[26–28]). However, it was observed that the gas-generation speeds tend to converge to the maximum value (over 20 μl/s) due to fast water absorption through the permeable bottom. To counteract this, it was found that upon the addition and even distribution of ethylcellulose (EC), which is an edible and biodegradable polymer[61] known to be hydrophobic, in powdered form in the reagent mixture, the gas-generation rate could be controllably lowered. Thus, assuming a fuel flow rate q identical to the gas-generation rate, the expected duration of fuel expulsion could be engineered to range from 8.47 (i.e., flow rate 23.02 μl/s) seconds to 100 (i.e., assuming flow rate 1.95 μl/s upon the addition of sufficient amount of ethylcellulose) seconds. Here, we define the predicted motion duration of the edible aquatic robot to be the same as the predicted fuel expulsion duration, although the actual motion duration is also affected by the acceleration and deceleration time of the edible aquatic robot.

Characterization

The boat-shaped bodies and fluidic actuators used for testing have average masses of 0.483 g and 0.603 g, respectively, resulting in an average total mass of 1.428 g per vessel (Fig. 4b) (including the mass of the fuel and gas-generation chemicals). The nutritional profile of the edible aquatic robot was assessed from the relative mass of the commercial feed pellet used to make the boat-shaped hull and of the other components (Supplementary Methods Section S6), resulting in a composition of 77.0% protein, 17.3% carbohydrate and 2.7% lipids (Fig. 4c). Compared to a typical commercial feed pellet sample[32] (Supplementary Methods Fig. S6), the edible aquatic robot contains all essential nutrition classes and has a similar carbohydrate percentage, but at least 30% more proteins and 8% less lipids due to the gelatin mass added for structural purpose. Despite these deviations from food pellets, the nutritional profile of the aquatic robot is suitable for consumption by predatory aquatic animals, with the ingredient composition being tunable for any specific future application scenario, thanks to the versatility of the manufacturing method. Since the fuel and the byproduct of the gas-generation reaction (sodium citrate) are likely to be released or dissipated into water prior to ingestion, they were not considered in the nutritional profile.

Twelve edible aquatic robots were completely manufactured, and their free motion characterized in a tank of 130 cm by 65 cm filled with water up to 8 cm. Motion tests were carried out by individually placing diverse edible aquatic robot samples on still water and measuring fuel expulsion and motion trajectories from video recordings (Fig. 4b, see section "Methods" for details). Water was completely replaced after each individual test to best ensure comparability of the results, although surface tension measurements (Supplementary Methods Section S7) showed that the water surface tension remained effectively unchanged (reduced only by 2.67%) even upon the dispersal of surfactant from up to three aquatic robots. The triggering time (time required for the gas-generation reaction to initiate) and expulsion time (time needed for the fuel reservoir to be emptied) were measured from video footage.

The average triggering time was 3.42 s (s.d. 1.50 s), with the average expulsion time 30.36 s (s.d. 11.14 s) for samples with 10 mg ethylcellulose mixed in the reaction chamber (faster samples, Fig. 4d red bars), and 69.00 s (s.d. 17.31 s) for samples with 20 mg ethylcellulose (slower samples, Fig. 4d blue bars). Both scenarios lie within the range predicted by the model. Notably, the aquatic robot samples did not follow regular and linear motion trajectories but exhibited versatile pseudo-random behavior in terms of motion direction and speed, generating various trajectories (Supplementary Methods Section S8). It is observed from the angular velocity data (Supplementary Methods Section S8) that the samples of type L and type R have a tendency to turn towards opposite directions (Fig. 4e). Since the samples generated curvilinear trajectories (Supplementary Material Section S8), the average speed was calculated by combining the linear velocity measured at the center of the edible aquatic robot with the angular velocity (Supplementary Methods Section S8). The average speed was 0.052 m/s and the average maximum speed was 0.098 m/s for the faster samples, whereas for the slower samples the average speed was 0.034 m/s and the average maximum speed was 0.075 m/s, which are within the desired range of 0.5–3 body lengths per second (Fig. 4f). Compared to model predictions, which afforded speeds between 0.032 and 0.111 m/s (Supplementary Methods Section S8), based on assumed fuel flow rates between 1.95 and 23.02 μl/s (see subsection "Fluidic actuator"), all samples exhibited expected average speed values within this range, considering the standard deviation, and there is a general trend of motion speed decrease with the increase of motion duration. Small deviations amongst individual samples were likely caused by the differences in mass and fuel reservoir volume of each sample, caused by manual fabrication imperfections, and also the inherent sim-to-real gap of the physical model. For example, a sample with a smaller mass would in reality be able to travel faster than the model could predict due to the reduced drag compared to the physical model (Supplementary Methods Section S1), as the model prediction is performed using the averaged mass value of all samples.

Discussion

In this article, we described, modeled, and characterized a fully edible robotic vessel capable of autonomously triggering self-propulsion for an extended period of time when placed on water. Additionally, we proposed a method for evaluating various surfactants to identify those that optimize self-propulsion while minimizing toxicity to aquatic fauna. The ingredient composition of the edible aquatic robot is tailored to meet the nutritional needs of cultivated predatory species, demonstrating its harmless nature and potential as an environmental sensing vessel or application as artificial prey. However, assessing the attractiveness and effectiveness of the proposed edible aquatic robot in the pet industry or animal research would require extensive animal testing and economic analysis, which fall beyond the scope of this study.

The edible aquatic robot samples were built manually according to the methods described here and in the Supplementary Materials, which induced imperfections in the different manufacturing steps. Although the results of the experimental characterization were mostly within the range of the model predictions, they did display some variability. The variability in fuel expulsion time was likely due to the actual concentration of the reagents, which was more precisely controllable in literature studies[22] but less precisely controllable in the manual assembly of the edible aquatic robot, and to manufacturing imperfections, such as small leakage points in the reaction chamber, that may have caused pressure loss. The variability in the pseudo-random curvilinear trajectories (instead of a more regular and linear trajectory) was likely due to small differences in fuel expulsion rate, hull shape, and water-vessel interaction in Marangoni-based propulsion systems[62]; however, trajectory variability is considered a positive feature because it would contribute to effective dispersion of the vessels on the water surface and possible increased attractiveness to predatory fish species whose natural prey display pseudo-random behavior[63–65]. Finally, the variability in the average and maximum speed was likely due to the combination effect of the irregular trajectory and imperfections in the shape of the fluidic channels and outlet, which could impact fuel supply efficiency η (Supplementary Methods Sections S1 and S4) and thus cause minor deviations from flow rate assumptions of the model, although all results were with the range predicted by the model when considering their standard deviations. Overall, higher fabrication efficiency and reduced variability could be achieved by the development of future versions of the edible aquatic robot optimized for more

controllable motions by using automated machine manufacturing for more precise control of ingredient composition, process duration, temperature, and humidity, and molding and sealing.

The edible aquatic robot surpassed conventional fish feed in two aspects. It contained 106.2 mL·kg^{-1} of propylene glycol on average, significantly higher than the 7.5 mL·kg^{-1} reported in the literature[58]. This increase resulted from the fuel reservoir's design, which maximized fuel volume (195 μl nominal) to extend motion duration, with no evidence suggesting harm to aquatic fauna. Additionally, the robot's vessel measured 47 mm in length, compared to the <14 mm diameter of commercial pellets[31,33]. However, some predatory fish naturally consume prey of similar or greater length[66]. If required for future practical applications, the robot's length could be adjusted by modifying the hull shape, though this would either reduce the motion speed or duration. In terms of locomotion speed, the edible aquatic robot achieved a peak speed (0.138 m/s) of nearly three times its body length and an average speed (0.052 m/s for samples with 0.2 mg EC) of approximately one body length. This performance is comparable to the state-of-the-art centimeter-scale aquatic robots. However, its controllability and maneuverability remain limited due to the minimal use of electronics.

The design, model, and methods described in this article could be applied to various types of aquatic applications, such as environmental monitoring with a swarm of edible aquatic robots, equipped with biodegradable and edible sensors[19,67], which would not harm aquatic fauna and also offer environmental advantages through end-of-life properties as feed, or if not eaten, biodegradability. Although here we did not carry out animal experiments, which would require ethical permissions and animal testing infrastructure, we speculate that the motion of these aquatic robots could possibly provide predatory training and cognitive stimulation[68] to aquatic pets, thus helping to reduce stress levels and ultimately enhance animal welfare[69,70]. More broadly, these results contribute to the recent trend in animation of processed food, which reconciles the motion of living natural prey with the nutritional balance of processed food for environmental, medical, and nutritional purposes[19].

Methods

Preparation of freeze-dried boat-shaped body samples: commercial feeding pellets (Dynamite Baits) were ground into powder using a spice grinder (WSG30, Waring). The liquid suspension that contained 25% w/v ingredients (including the ground feed, the edible binder: gelatin (Sigma-aldrich), starch (potato source, Patissier) or flour (wheat source, Migros), and optionally the hydrophobic additives: fish oil (KoRo), shellac (Kremer Pigmente) or beeswax (Sky Organics), depending on the specific recipe) dispersed in water was prepared by heating the suspension in a beaker to 90 °C with constant manual stirring for 15 min. The temperature and duration were selected through preliminary tests to allow all the ingredients to be melted and form an evenly dispersed mixture. The mixture was then poured onto silicone rubber (Smooth On Inc., Smooth-Sil 940) molds, cooled to ambient temperature, then frozen at −30 °C for at least 6 h and loaded into the freeze drier (Christ Epsilon 2-10D, Martin Christ) and went through a drying procedure of 72 h, where the freezing temperature and drying time were selected according to common practice in the literature[71] to allow slow and uniform sublimation of moisture from the structure, ensuring uniform and even product structure.

Test of freeze-dried boat-shaped body samples: to test the water absorption rate of the samples, a weight scale capable of real-time data recording (Explorer Precision, Ohaus) was used. The samples were secured under a height-adjustable test platform, and the height was adjusted to allow marginal contact between the sample and the water surface in a beaker. The beaker was placed on the measuring plate of the weight scale to allow real-time monitoring of the weight change during the water absorption process. The texture strength of the samples was tested by 3-point bending experiments on a texture analyzer (Instron) and evaluated by flexural modulus on specifically prepared rectangular shape samples with an intersection size 4 × 15 mm and a support distance 30 mm.

Fabrication of the fluidic actuator: gelatin (porcine skin source, gel strength 170–195 g bloom, Sigma-Aldrich) and glycerol (Abcr GmbH) were used as received. A 33% w/w gelatin solution was prepared by mixing gelatin, water, and glycerol in a threaded cap bottle, with a 4:1 mass ratio between gelatin and glycerol. The bottle was then sealed and incubated in an oven for at least 8 h at 60 °C to form a clear solution. The solution was then carefully cast onto the silicone rubber (Smooth On Inc., Smooth-Sil 940) molds for the top and bottom fluidic layers and detachable reaction chamber wall (Fig. 1b) and left to cool down to room temperature, allowing a firm hydrogel to form. The hydrogel was left on the mold, held by 3D-printed plastic fixtures, and dried at ambient temperature (23 °C–26 °C) and humidity (relative humidity 23 ± 3%) for 12 h. Then, cellulose filter paper (Whatman, grade 597, thickness 180 μm) was glued with gelatin solution to the reaction chamber's bottom and dried together to form a firm connection. The top fluidic layer and bottom fluidic layer were then bound by applying 20% w/v transglutaminase (Moo Gloo) solution, and dried for another 6 h in 3D-printed fixtures to form an airtight connection while maintaining a flat shape. 5% w/v ethylcellulose (~50 cP, Carl Roth GmbH & Co. Kg) solution in isopropanol alcohol (99%, Thommen Furler AG) was then injected into the fuel reservoir of the fluidic actuator and subsequently emptied with pressurized gas purging. The fluidic actuator was then allowed to dry for another 4 h, allowing a thin hydrophobic coat to form inside the reservoir, thus inhibiting the gelatin structure from absorbing the fuel (propylene glycol). Next, the fuel propylene glycol, mixed with 0.5% by weight blue food dye (Zhongshan Jiupin Food Co.) for visualization, was injected into the fuel reservoir using a syringe pump (CETONI, Nemesys). Citric acid (Fluorochem), sodium bicarbonate (Migros) and ethylcellulose (~50 cP, Carl Roth GmbH & Co. Kg) were then measured by a weight scale (Denver Instrument MXX-123), mixed thoroughly and loaded into the detachable reaction chamber, which was subsequently mechanically connected to the bottom fluidic layer and sealed with oleogel sealant (one part of beeswax (Sky Organics) and two parts olive oil (Monini) by mass, hot melt mixed at 75 °C).

Motion tests: liquid lecithin (Now Foods, phosphorus concentration 17 mg/mL), propylene glycol (MP Biomedicals), and ethanol (99.8%, Fisher Scientific) were used as received. Edible aquatic robot locomotion experiments in subsection "Characterization" were carried out in a portable water pool with a size of 130 × 65 cm and water depth 8 cm, rotary vessel locomotion tests in subsection "Fuel selection" were carried out in the same container with water depth 3.5 cm. Circular colored paper tape cuts were attached to the test vessels, enabling vision motion tracking through video record. Videos were captured by a Sony IMX 586 digital camera (30 FPS) and processed by motion tracking software (Tracker) to acquire the position and time stamp data, and manually measured to read the triggering time and expulsion duration of the fluidic actuators. The position and time stamp data were then processed in data analysis software (MATLAB) to acquire the trajectory and speed information.

Data availability

All (other) data needed to evaluate the conclusions in the paper are present in the paper or the Supplementary Materials. The data for this study have been deposited in the database at https://doi.org/10.5281/zenodo.14933645.

References

1. Bayat, B., Crespi, A. & Ijspeert, A. Envirobot: a bio-inspired environmental monitoring platform. In *Proc. 2016 IEEE/OES Autonomous Underwater Vehicles (AUV)* 381–386. https://doi.org/10.1109/AUV.2016.7778700 (2016).
2. Bogue, R. The role of robots in environmental monitoring. *Industrial Robot* **50**, 369–375 (2023).

3. Katzschmann, R. K., DelPreto, J., MacCurdy, R. & Rus, D. Exploration of underwater life with an acoustically controlled soft robotic fish. *Sci. Robot.* **3**, eaar3449 (2018).
4. Spino, P. & Rus, D. Towards centimeter-scale underwater mobile robots: an architecture for capable μAUVs. In *Proc. 2024 IEEE International Conference on Robotics and Automation (ICRA)* 1484–1490. https://doi.org/10.1109/ICRA57147.2024.10610474 (2024).
5. Hartmann, F. et al. Highly agile flat swimming robot. *Sci. Robot.* **10**, eadr0721 (2025).
6. Li, K. et al. A 5 cm-scale piezoelectric jetting agile underwater robot. *Adv. Intell. Syst.* **5**, 2200262 (2023).
7. Chen, Y., Doshi, N., Goldberg, B., Wang, H. & Wood, R. J. Controllable water surface to underwater transition through electrowetting in a hybrid terrestrial-aquatic microrobot. *Nat. Commun.* **9**, 2495 (2018).
8. Li, G. et al. Self-powered soft robot in the Mariana Trench. *Nature* **591**, 66–71 (2021).
9. Ko, J. et al. High-performance electrified hydrogel actuators based on wrinkled nanomembrane electrodes for untethered insect-scale soft aquabots. *Sci. Robot.* **7**, eabo6463 (2022).
10. Wang, D. et al. Miniature amphibious robot actuated by rigid-flexible hybrid vibration modules. *Adv. Sci.* **9**, 2203054 (2022).
11. Lauga, E. & Davis, A. M. J. Viscous Marangoni propulsion. *J. Fluid Mech.* **705**, 120–133 (2012).
12. Kwak, B., Choi, S., Maeng, J. & Bae, J. Marangoni effect inspired robotic self-propulsion over a water surface using a flow-imbibition-powered microfluidic pump. *Sci. Rep.* **11**, 17469 (2021).
13. Song, S. W. et al. Pen-drawn Marangoni swimmer. *Nat. Commun.* **14**, 3597 (2023).
14. Sharma, R., Chang, S. T. & Velev, O. D. Gel-based self-propelling particles get programmed to dance. *Langmuir* **28**, 10128–10135 (2012).
15. Pena-Francesch, A., Giltinan, J. & Sitti, M. Multifunctional and biodegradable self-propelled protein motors. *Nat. Commun.* **10**, 3188 (2019).
16. Mao, J., Han, D., Zhou, H., Sun, H. & Zhang, Y. Bioinspired superhydrophobic swimming robots with embedded microfluidic networks and photothermal switch for controllable *Marangoni* propulsion. *Adv. Funct. Mater.* **33**, 2208677 (2023).
17. Sethi, S. S., Kovac, M., Wiesemüller, F., Miriyev, A. & Boutry, C. M. Biodegradable sensors are ready to transform autonomous ecological monitoring. *Nat. Ecol. Evol.* **6**, 1245–1247 (2022).
18. Qi, Q. et al. The rise of transient robotics. *Device* **2**, 100554 (2024).
19. Floreano, D. et al. Towards edible robots and robotic food. *Nat. Rev. Mater.* https://doi.org/10.1038/s41578-024-00688-9 (2024).
20. Trevathan, J. & Johnstone, R. Smart environmental monitoring and assessment technologies (SEMAT)—a new paradigm for low-cost, remote aquatic environmental monitoring. *Sensors* **18**, 2248 (2018).
21. Hughes, J. & Rus, D. Mechanically programmable, degradable & ingestible soft actuators. In *Proc. 2020 3rd IEEE International Conference on Soft Robotics (RoboSoft)* 836–843. https://doi.org/10.1109/RoboSoft48309.2020.9116001 (IEEE, 2020).
22. Okui, M., Nagura, Y., Iikawa, S., Yamada, Y. & Nakamura, T. A pneumatic power source using a sodium bicarbonate and citric acid reaction with pressure booster for use in mobile devices. In *Proc. 2017 IEEE/RSJ International Conference on Intelligent Robots and Systems (IROS)* 1040–1045. https://doi.org/10.1109/IROS.2017.8202272 (IEEE, 2017).
23. Khajepour, F. & Hosseini, S. A. Citric acid improves growth performance and phosphorus digestibility in Beluga (Huso huso) fed diets where soybean meal partly replaced fish meal. *Anim. Feed Sci. Technol.* **171**, 68–73 (2012).
24. Guo, Z. et al. Dietary citric acid improves growth performance, feed utilization, phosphorus utilization, lateral scute hardness, and duodenal microstructure in juvenile hybrid sturgeon (Acipenser baerii ♀ × A. schrenckii ♂). *Aquac. Rep.* **33**, 101833 (2023).
25. Hasimuna, O. J., Monde, C., Bbole, I., Maulu, S. & Chibesa, M. The efficacy of sodium bicarbonate as an anaesthetic agent in Oreochromis macrochir juveniles. *Sci. Afr.* **11**, e00668 (2021).
26. Romano, N. et al. Dietary sodium citrate improved oxidative stability in red hybrid tilapia (Oreochromis sp.) but reduced growth, health status, intestinal short chain fatty acids and induced liver damage. *Aquaculture* **458**, 170–176 (2016).
27. Sotoudeh, E., Saghaei, S. & Dehghani, M. Effects of dietary sodium citrate on growth performance, body composition and digestive enzymes activity of yellowfin seabream (Acanthopagrus latus) fingerling. *Aquac. Sci.* **8**, 32–42 (2020).
28. Wang, J.-X. et al. Double-edged effect of sodium citrate in Nile tilapia (Oreochromis niloticus): promoting lipid and protein deposition vs. causing hyperglycemia and insulin resistance. *Anim. Nutr.* **14**, 303–314 (2023).
29. Tudorache, C., O'Keefe, R. A. & Benfey, T. J. Optimal swimming speeds reflect preferred swimming speeds of brook charr (Salvelinus fontinalis Mitchill, 1874). *Fish. Physiol. Biochem.* **37**, 307–315 (2011).
30. Suematsu, N. J., Sasaki, T., Nakata, S. & Kitahata, H. Quantitative estimation of the parameters for self-motion driven by difference in surface tension. *Langmuir* **30**, 8101–8108 (2014).
31. Mattila, J. & Koskela, J. Effect of feed pellet size on production parameters of pike-perch (*Sander lucioperca*). *Aquac. Res.* **49**, 586–590 (2018).
32. Craig, S. R., Helfrich, L. A., Kuhn, D. & Schwarz, M. H. Understanding fish nutrition, feeds, and feeding. *Virginia Coop. Ext.* 420–256 (2017).
33. Khater, E. S. G., Bahnasawy, A. H. & Ali, S. A. Physical and mechanical properties of fish feed pellets. *J. Food Process. Technol.* **5**, 1–6 (2014).
34. Baudron, V., Gurikov, P., Smirnova, I. & Whitehouse, S. Porous starch materials via supercritical- and freeze-drying. *Gels* **5**, 12 (2019).
35. Cheng, M., Zhang, D., Zhang, S., Wang, Z. & Shi, F. Tackling the short-lived marangoni motion using a supramolecular strategy. *CCS Chem.* **1**, 148–155 (2019).
36. Jin, H., Marmur, A., Ikkala, O. & Ras, R. H. A. Vapour-driven Marangoni propulsion: continuous, prolonged and tunable motion. *Chem. Sci.* **3**, 2526 (2012).
37. OECD (Organisation for Economic Co-operation and Development). *Test No. 202: Daphnia Sp. Acute Immobilisation Test*. https://doi.org/10.1787/9789264069947-en (accessed: May 2025).
38. OECD (Organisation for Economic Co-operation and Development). *Test No. 211: Daphnia Magna Reproduction Test*. https://doi.org/10.1787/9789264185203-en (accessed: May 2025).
39. OECD (Organisation for Economic Co-operation and Development). *Screening Information Dataset (SIDS) Initial Assessment Report for Ethanol (CAS No. 64-17-5)*. https://hpvchemicals.oecd.org/ui/handler.axd?id=2602cc56-d998-4e67-bd78-5454ef3f8f9a (accessed: May 2025).
40. OECD (Organisation for Economic Co-operation and Development). *Screening Information Dataset (SIDS) Initial Assessment Report for 1,2-Dihydroxypropane (CAS No. 57-55-6)*. https://hpvchemicals.oecd.org/ui/handler.axd?id=8ff27582-80e7-472a-8e86-f57aea93ffff (accessed: May 2025).
41. European Chemicals Agency (ECHA). Methyl hexanoate registration dossier. https://chem.echa.europa.eu/100.003.115/ (accessed: May 2025).
42. European Chemicals Agency (ECHA). 3-methylbutan-1-ol registration dossier. https://chem.echa.europa.eu/100.004.213/ (accessed: may 2025).
43. European Chemicals Agency (ECHA). L-menthol registration dossier. https://chem.echa.europa.eu/100.016.992/ (accessed: May 2025).
44. European Chemicals Agency (ECHA). Dehydrated sorbitol, C18 (unsaturated) fatty acid esters, ethoxylated registration dossier. https://chem.echa.europa.eu/100.252.233/ (accessed: May 2025).

45. Mondellini, S. et al. Beyond microplastics: water soluble synthetic polymers exert sublethal adverse effects in the freshwater cladoceran Daphnia magna. *Sci. Total Environ.* **847**, 157608 (2022).
46. Johann, S. et al. Mechanism-specific and whole-organism ecotoxicity of mono-rhamnolipids. *Sci. Total Environ.* **548–549**, 155–163 (2016).
47. European Chemicals Agency (ECHA). Phosphatidylcholines, soya, hydrogenated registration dossier. https://chem.echa.europa.eu/100.096.816/ (accessed: May 2025).
48. Vazquez, G., Alvarez, E. & Navaza, J. M. Surface tension of alcohol water + water from 20 to 50.degree. C. *J. Chem. Eng. Data* **40**, 611–614 (1995).
49. Hoke, B. C. & Patton, E. F. Surface tensions of propylene glycol + water. *J. Chem. Eng. Data* **37**, 331–333 (1992).
50. Vogel, A. I. Physical properties and chemical constitution. Part XIII. Aliphatic carboxylic esters. *J. Chem. Soc.* 624–644 (1948).
51. Jasper, J. J. The surface tension of pure liquid compounds. *J. Phys. Chem. Ref. Data* **1**, 841–1010 (1972).
52. Lewandowski, A. & Szymczyk, K. Adsorption of monoterpene alcohols at the water–air interface. *Adsorption* **25**, 301–308 (2019).
53. Pogorzelski, S., Watrobska-Swietlikowska, D. & Sznitowska, M. Surface tensometry studies on formulations of surfactants with preservatives as a tool for antimicrobial drug protection characterization. *J. Biophys. Chem.* **3**, 324–333 (2012).
54. Ospanova, Z., Mussabekov, K. B., Aidarova, S. B., Miller, R. & Asadov, M. Surface tension time and concentration dependencies of multifarious surfactants-based systems containing Polyvynyl alcohol. *J. Chem. Technol. Metall.* **54**, 503–507 (2019).
55. Beiranvand, F., Najibi, S. H., & Hashemi Shahraki, B. Experimental measurement of equilibrium surface tension of an aqueous solution of polyethylene glycol and a surfactant. *Iran. J. Oil Gas Sci. Technol.* **9**, 26–43 (2020).
56. Rocha, V. A. L. et al. Comparison of mono-rhamnolipids and di-rhamnolipids on microbial enhanced oil recovery (MEOR) applications. *Biotechnol. Prog.* **36**, e2981 (2020).
57. Vargaftik, N. B., Volkov, B. N. & Voljak, L. D. International tables of the surface tension of water. *J. Phys. Chem. Ref. Data* **12**, 817–820 (1983).
58. Soaudy, M. R. et al. Possibility mitigation of cold stress in Nile tilapia under biofloc system by dietary propylene glycol: Performance feeding status, immune, physiological responses and transcriptional response of delta-9-desaturase gene. *Aquaculture* **538**, 736519 (2021).
59. Liu, D., Nikoo, M., Boran, G., Zhou, P. & Regenstein, J. M. Collagen and gelatin. *Annu. Rev. Food Sci. Technol.* **6**, 527–557 (2015).
60. Gullapalli, R. P. & Mazzitelli, C. L. Gelatin and non-gelatin capsule dosage forms. *J. Pharm. Sci.* **106**, 1453–1465 (2017).
61. EFSA Panel on Additives and Products or Substances used in Animal Feed (FEEDAP) et al. Safety and efficacy of ethyl cellulose for all animal species. *EFSA J.* **18**, e06210 (2020).
62. Burton, L. J., Cheng, N. & Bush, J. W. M. The cocktail boat. *Integr. Comp. Biol.* **54**, 969–973 (2014).
63. Matsunaga, W. & Watanabe, E. Visual motion with pink noise induces predation behaviour. *Sci. Rep.* **2**, 219 (2012).
64. Ioannou, C. C., Carvalho, L. A. B., Budleigh, C. & Ruxton, G. D. Virtual prey with Lévy motion are preferentially attacked by predatory fish. *Behav. Ecol.* **34**, 695–699 (2023).
65. Pohlmann, K., Grasso, F. W. & Breithaupt, T. Tracking wakes: the nocturnal predatory strategy of piscivorous catfish. *Proc. Natl. Acad. Sci. USA* **98**, 7371–7374 (2001).
66. Hilborn, R. et al. When does fishing forage species affect their predators? *Fish. Res.* **191**, 211–221 (2017).
67. Sharova, A. S., Melloni, F., Lanzani, G., Bettinger, C. J. & Caironi, M. Edible electronics: the vision and the challenge. *Adv. Mater. Technol.* **6**, 2000757 (2021).
68. Kleiber, A. et al. Cognitive enrichment to increase fish welfare in aquaculture: a review. *Aquaculture* **575**, 739654 (2023).
69. Sundström, L. F. & Johnsson, J. I. Experience and social environment influence the ability of young brown trout to forage on live novel prey. *Anim. Behav.* **61**, 249–255 (2001).
70. Tudorache, C., de Boeck, G. & Claireaux, G. Forced and preferred swimming speeds of fish: a methodological approach. in *Swimming Physiology of Fish: Towards Using Exercise to Farm a Fit Fish in Sustainable Aquaculture* (eds Palstra, A. P. & Planas, J. V.) 81–108. https://doi.org/10.1007/978-3-642-31049-2_4 (Springer Berlin Heidelberg, 2013).
71. Zhu, R., Schutyser, M. A. I., Boom, R. M. & Zhang, L. Tuning the mechanical properties of starch-based cryogels with the aid of additives. *Carbohydr. Polym. Technol. Appl.* **8**, 100548 (2024).

Acknowledgements

The authors thank Y. Sun, Y. Piskarev, and H.V. Phan for valuable discussions and comments on the manuscript; E. Schreuder, M. Strubel, G. Cocchi, and Z. Saraw for the kind arrangement of experiments. Figure 3a used community-contributed code "symlog" function by R. Perrotta. This work as funded by the European Union's Horizon 2020 research and innovation program under grant agreement 964596 ROBOFOOD.

Author contributions

B.K. and D.F. initiated the concept. S.Z., B.K., R.Z., and D.F. designed the research. S.Z., R.Z., and B.K. conducted the experiments. L.Z., R.M.B., and D.F. supervised the project and acquired the funding. S.Z., R.Z., B.K., M.P., L.Z., and D.F. wrote the manuscript.

Competing interests

The authors declare no competing interests.

Additional information

Supplementary information The online version contains supplementary material available at https://doi.org/10.1038/s41467-025-59559-8.

Correspondence and requests for materials should be addressed to Dario Floreano.

Peer review information *Nature Communications* thanks Alireza Fath, and the other, anonymous, reviewer(s) for their contribution to the peer review of this work. A peer review file is available.